Published in final edited form as:
Nanomedicine (Lond). 2009 December ; 4(8): 903–917. doi:10.2217/nnm.09.71.

NanoART synthesis, characterization, uptake, release and toxicology for human monocyte—macrophage drug delivery

Ari S Nowacek[1,*], **Reagan L Miller**[2,*], **JoEllyn McMillan**[1], **Georgette Kanmogne**[1], **Michel Kanmogne**[1], **R Lee Mosley**[1], **Zhiya Ma**[1], **Sabine Graham**[2], **Mahesh Chaubal**[2], **Jane Werling**[2], **Barrett Rabinow**[2], **Huanyu Dou**[1], and **Howard E Gendelman**[1,†]

[1]Department of Pharmacology & Experimental Neuroscience, University of Nebraska Medical Center, Omaha, NE 68198-5880, USA

[2]Baxter Healthcare Corporation, Round Lake, IL 60073, USA

Abstract

Background—Factors limiting the efficacy of conventional antiretroviral therapy for HIV-1 infection include treatment adherence, pharmacokinetics and penetration into viral sanctuaries. These affect the rate of viral mutation and drug resistance. In attempts to bypass such limitations, nanoparticles containing ritonavir, indinavir and efavirenz (described as nanoART) were manufactured to assess macrophage-based drug delivery.

Methods—NanoART were made by high-pressure homogenization of crystalline drug with various surfactants. Size, charge and shape of the nanoparticles were assessed. Monocyte-derived macrophage nanoART uptake, drug release, migration and cytotoxicity were determined. Drug levels were measured by reverse-phase high-performance liquid chromatography.

Results—Efficient monocyte-derived macrophage cytoplasmic vesicle uptake in less than 30 min based on size, charge and coating was observed. Antiretroviral drugs were released over 14 days and showed dose-dependent reduction in progeny virion production and HIV-1 p24 antigen. Cytotoxicities resulting from nanoART carriage were limited.

Conclusion—These results support the continued development of macrophage-mediated nanoART carriage for HIV-1 disease.

Keywords

antiretroviral therapy; antiviral response; HIV; monocyte-derived macrophage; nanoART; nanoparticle

Although antiretroviral therapy (ART) has greatly reduced disease morbidity and mortality in HIV-1-infected people, a major limitation for treatment is the need for lifelong daily drug dosing. To achieve sustained viral suppression, maintenance of therapeutic drug levels is required [1–4]. Thus, suboptimal adherence causes increased risk for treatment failure and viral resistance [5]. Moreover, penetration of drugs into viral tissue sanctuaries, such as the CNS, is also limited by oral ART, leading to diminished therapeutic efficacy reflected in cognitive dysfunction and accelerated disease [6–11]. In addition, substance abuse, common among

†Author for correspondence: Department of Pharmacology & Experimental Neuroscience, University of Nebraska Medical Center, Omaha, NE 68198-5880, USA Tel.: +1 402 559 8920; Fax: +1 402 559 3744; hegendel@unmc.edu.
*Both authors contributed equally to this work.

No writing assistance was utilized in the production of this manuscript.

HIV-1-infected individuals, has long been recognized as a risk factor for poor therapeutic adherence [12]. As a result, healthcare providers are often reluctant to prescribe ART to patients who illicitly use drugs because of promotion of virologic resistance and accelerated viral transmission [13,14]. Adding to such concerns, ART is not yet available to all who need it, most notably those in resource-limited settings [15,16].

Thus, our laboratories have embarked on the development of nanoformulated ART aimed at virus target tissues and improved drug delivery. As monocytes and monocyte-derived macrophages (MDM) are cellular reservoirs for HIV and have the ability to uptake, transport and release ART into infected tissues, these cells were proposed as drug carriers [17–19]. Although such formulations were controlled for stability, early studies showed limitations in both cellular uptake and release, which necessitated *ex vivo* loading of monocytes and MDM followed by adoptive transfer in order to reach therapeutic end points. Indeed, the promise and perils for such nanotargets were reported previously in laboratory and animal models of human disease [20]. With this in mind, we tested just such a drug-delivery approach adjusting for surfactant composition, size and charge. These enabled efficient development of nanoformulated antiretroviral drugs, collectively referred to as nanoART. Optimization of drug loading and release was done by pharmacokinetic and antiretroviral nanoART measurements. Cell entry and release of ritonavir (RTV), indinavir (IDV) and efavirenz (EFV) nanoparticles (NPs) were optimized based on size, coating and charge. Reverse-phase high-performance liquid chromatography (RP-HPLC) showed uptake of drugs into cells of 1 log or more or above the EC_{50} without cytotoxicity and sustained drug release for up to 15 days. Antiretroviral efficacy was determined by infecting MDM with HIV-1_{ADA} (a macrophage tropic viral strain) every 5 days for up to 15 days following nanoART treatment. NanoART-loaded cells showed sustained antiretroviral activities for many of the formulations tested. These results provide proof-of-concept that ART compounds can be manufactured into stable NPs that can be targeted to cells and used in cell-mediated drug-delivery systems. These data also suggest that nanoART may be developed for human use to improve dosing schedule, optimize adherence and increase therapeutic efficacy for HIV-1 disease.

Materials & methods

Preparation & characterization of nanoART

NanoART of IDV, RTV and EFV were prepared by high-pressure homogenization using an Avestin C-5 homogenizer (Avestin, Inc., Ottawa, ON, Canada). A range of surfactants were used to coat the drug crystals including Lipoid E80® (an egg phosphatide mixture of phosphatidylcholine, phosphatidylethanoloamine and the hydrolyzed lyso [single aliphatic chain]; Lipoid GmbH, Ludwigshafen, Germany), a block copolymer of ethylene oxide and propylene oxide (poloxamer 188 [P-188]; Spectrum Chemicals, Gardena, CA, USA), 1,2-distearoyl-phosphatidyl-ethanolamine-methyl-poly(ethylene-glycol) (DSPE-$mPEG_{2000}$; Genzyme, Cambridge, MA, USA), poly(lactic-co-glycolic acid) (PLGA; ratio 50:50 of lactide to glycolide; Sigma-Aldrich, St Louis, MO, USA), (1-oleoyl-2-[6-[(7-nitro-2–1,3-benzoxadiazol-4-yl)amino]hexanoyl]-3-trimethylammonium propane) (DOTAP; Genzyme) and cetyltrimethyl ammonium bromide (CTAB; Sigma-Aldrich). To coat the nanosized drug crystals, either alone or in combination, each surfactant (or copolymer) (weight/weight percent) was made up of Lipoid E80 (1.4%), P-188 (0.5%), DSPE -$mPEG_{2000}$ (0.2%), PLGA (12%), DOTAP (0.1%) and CTAB (0.5%). The nanosuspensions were formulated at a slightly alkaline pH of 7.8 using either 10 mM sodium phosphate or 10 mM HEPES as a buffer. Tonicity was adjusted with glycerin (2.25%) or sucrose (9.25%). Drug was added to the surfactant solution to make a concentration of approximately 2% (weight-to-volume ratio [%]). Lissamine rhodamine B 1,2-dihexadecanoyl-*sn*-glycero-3-phosphoethanolamine, triethylammonium salt (rDHPE; Invitrogen, Carlsbad, CA, USA) was used to label nanoART, which appeared as red

fluorescence. In order to synthesize nanoART, a suspension was prepared by adding crystalline drug to a surfactant solution and mixing for 4–7 min using an Ultra-Turrax T-18 (IKA® Works Inc., Wilmington, NC, USA) rotor-stator mixer to reduce initial particle size. The suspension was homogenized at 20,000 pounds per square inch for approximately 30 passes or until desired particle size was reached. For DOTAP-containing suspensions, the homogenized suspension was centrifuged (12,100 × g for 30 min at 5°C) to pellet the drug particles. The supernatant was decanted and surfactant-containing DOTAP was added to the drug pellet. The drug was resuspended by mixing with an Ultra-Turrax T-18.

In the case of EFV–PLGA NPs, EFV (1.25 g) and PLGA (6 g) were dissolved in dichloromethane (50 ml) and added to a 1% poly(vinyl) alcohol solution (500 ml). Particle size was achieved by sonicating at 50% amplitude for 10 min using a 400/600 W sonicator with a ¾ inch high gain probe. The solution was stirred overnight to evaporate the dichloromethane-hardened particles. The suspension was then centrifuged, washed with 18-Ω water and decanted twice. The particles were suspended in 10% mannitol before being frozen or lyophilized for storage. For all nanosuspensions, particle size was measured using a HORIBA LA 920 light scattering instrument (HORIBA Instruments Inc., Irvine, CA, USA; RRI = 1.08 for IDV and 1.20 for RTV and EFV). ζ-potential was measured by diluting 0.1 ml of the suspension into 9.9 ml of 10 mM HEPES, pH 7.4 on a Malvern Zetasizer Nano series instrument (Malvern Instruments Inc., Westborough, MA, USA). Final drug content of the formulations was determined by RP-HPLC (data not shown).

Human monocyte isolation & cultivation

Human monocytes were obtained by leukapheresis from HIV-1 and hepatitis seronegative donors and were purified by counter-current centrifugal elutriation [17]. Wright-stained cytospins were prepared and cell purity assayed by immunolabeling with anti-CD68 (clone KP-1). Monocytes were cultivated at a concentration of 1×10^6 cells/ml at 37°C in a humidified atmosphere (5% CO_2) in Dulbecco's modified Eagle medium supplemented with 10% heat-inactivated pooled human serum, 1% glutamine, 50 μg/ml gentamicin, 10 μg/ml ciprofloxacin and 1000 U/ml recombinant human macrophage colony stimulating factor, a generous gift of Wyeth Inc. (Cambridge, MA, USA). To induce differentiation to macrophages, monocytes were cultured for 7 days in the presence of macrophage colony stimulating factor [21].

Electron microscopy

Samples were fixed with 3% glutaraldehyde in 0.1 M phosphate buffer (pH 7.4) and further fixed in 1% osmium tetroxide in 0.1 M phosphate buffer (pH 7.4) for 1 h. Samples were dehydrated in a graduated ethanol series and embedded in Epon 812 (Electron Microscopic Sciences, Fort Washington, PA, USA) for scanning-electron microscopy. Thin sections (80 nm) were stained with uranyl acetate and lead citrate and observed under a transmission electron microscope (Hitachi H7500-I; Hitachi High Technologies America Inc., Schaumburg, IL, USA).

NanoART uptake & release

Monocyte-derived macrophages (2×10^6 per well) were cultured with nanoART at concentrations of 1, 10 and 100 μM. Uptake of nanoART was assessed without medium change for 24 h with cell collection occurring hourly. Adherent MDM were collected by washing three times with 1 ml of phosphate-buffered saline, followed by scraping cells into 1 ml phosphate-buffered saline. Samples were centrifuged at 950 × g for 10 min at 4°C, and the supernatant removed. Cell pellets were sonicated in 200 μl of methanol and centrifuged at 10,000 × g for 10 min at 4°C. The methanol extract was stored at −80°C until RP-HPLC analysis was performed.

After an initial 12 h exposure to nanoART, drug release from MDM with half media exchanges every other day was evaluated over a 2-week period. Media samples were saved along with replicate cells and stored at −80°C until RP-HPLC analysis could be performed using a modified version of a previously published method [18]. Methanol-extracted cell suspensions were centrifuged at 21,800 × g at 4°C for 10 min. Media samples were thawed and deproteinated by the addition of methanol. The samples were centrifuged at 21,800 × g at 4°C for 10 min; supernatants evaporated to dryness under vacuum and were resuspended in 70 μl of 100% methanol. Triplicate 20 μl samples of processed media or cells were assessed by RP-HPLC using a YMC Pack Octyl C8 column (Waters Inc., Milford, MA, USA) with a C8 guard cartridge. Mobile phase consisting of 47% acetonitrile/53% 25mM KH_2PO_4, pH 4.15 (adjusted with 1 N HCl) was pumped at 0.4 ml/min with UV/Vis detection at 212 nm. For all antiretroviral drugs, quantitations were assessed by comparison to a standard curve of free drug (0.025–100 μg/ml) made in methanol.

Antiretroviral activities of nanoART

Monocyte-derived macrophages were treated with 1, 10 or 100 μM of nanoART for 12 h, washed to remove excess drug and infected with HIV-1_{ADA} at a multiplicity of infection of 0.01 infectious viral particles/cell [21] on days 1, 5, 10 and 15 after treatment. Following viral infection, cells were cultured for 10 days with half media exchanges every other day. Media samples were collected on days 5, 7 and 10 for measurement of progeny virion production, as assayed by RT activity [22]. Parallel analyses for expression of HIV-1 p24 antigen by infected cells were performed by immunostaining on day 10 postinfection.

RT assays

In a 96-well plate, media samples (10 μl) were mixed with 10 μl of a solution containing 100 mM Tris-HCl (pH 7.9), 300 mM KCl, 10 mM DTT, 0.1% nonyl phenoxylpolyethoxy-lethanol-40 and water. The reaction mixture was incubated at 37°C for 15 min and 25 μl of a solution containing 50 mM Tris-HCl (pH 7.9), 150 mM KCl, 5 mM DTT, 15 mM $MgCl_2$, 0.05% nonyl phenoxylpolyethoxy-lethanol-40, 10 μg/ml poly(A), 0.250 U/ml oligo d $(T)_{12–18}$ and 10 μCi/ml ^{3}H-TTP was added to each well; plates were incubated at 37°C for 18 h. Following incubation, 50 μl of cold 10% TCA was added to each well, the wells were harvested onto glass fiber filters and the filters were assessed for ^{3}H-TTP incorporation by β-scintillation spectropmetry using a TopCount NXT (PerkinElmer Inc., Waltham, MA, USA) [22].

Live cell confocal microscopy

Monocyte-derived macrophages were stained using Vybrant DiO cell-labeling solution and viable MDM were identified by green fluorescence. NPs were labeled with rDHPE by adding fluorescent phospholipid. rDHPE-labeled NPs (rDHPE-nanoART) exhibited a red fluorescence. Based on the amount of tracer added, the number of labeled phospholipid molecules represents a very small fraction of the total coating material and contributes minimally to the thickness of the phospholipid coating. This was confirmed by size measurements that showed no significant differences in the sizes of nanoART formulated with or without rDHPE phospholipid (data not shown). In addition, no differences were detected in the uptake or the release of drug formulated with the fluorescent phospholipid compared with unlabeled particles. For representative formulations tested, more than 95% of MDM had taken up rDHPE-nanoART after 12 h of incubation (data not shown). Images were captured every 30 s using a Nikon TE2000-U (Nikon Instruments Inc., Melville, NY, USA) with swept-field confocal microscrope 488 nm (green) and 568 nm (red) laser excitations, and a 60× objective.

Immunohistochemistry

Cells were fixed with 4% phosphate-buffered paraformaldehyde 10 days after HIV-1 infection. Mouse monoclonal antibodies to HIV-1 p24 (1:10, Dako, Carpinteria, CA, USA) were used to determine the density of HIV-1-infected cells. Quantification of immunostaining was performed by densitometry using Image-Pro Plus, v. 4.0 (Media Cybernetics Inc., Bethesda, MD, USA). Expression of p24 was quantified by determining the positive area (index) as a percentage of the total image area per microscopy field [17].

Cytotoxicity

To determine any potential toxic effects of NPs on cells, monocytes and MDM were treated with 100 μM of NPs for 12 h, and cytotoxicity assessed over 24 h using alamarBlue™ assay (AbD Serotec, Raleigh, NC, USA) according to the manufacturer's instructions [23].

Transendothelial migration assay

Monocyte migration across the blood–brain barrier was performed as previously described [24,25]. For this assay, 2×10^4 human brain microvessel endothelial cells (HBMECs) were seeded on collagen-coated FluoroBlok™ tinted tissue culture inserts (3 μm pore size) from BD Biosciences (Franklin Lakes, NJ, USA). Because HBMEC monolayers are not visible on these inserts, manual readings of trans-epithelial electric resistance were assessed with an EVOM voltmeter (World Precision Instruments, Sarasota, FL, USA) to confirm monolayer formation and confluence. Monocytes were labeled with calcein-AM (Invitrogen) at 5 μM/1×10^6 cells for 45 min and washed with phosphate-buffered saline. For migration, 2.5×10^5 labeled monocytes were placed on HBMEC monolayers (upper chamber of the FluoroBlok insert) and allowed to migrate across the monolayer for 2 h (37°C, 5% CO_2). Monocytes migrating into the lower chamber were quantified using a fluorescence plate reader (absorbance: 494 nm; emission: 517 nm) and compared with a standard curve derived from a serial dilution of a known number of calcein-labeled cells.

Statistical analyses

Statistical Analysis Software (SAS Institute, Inc., Cary, NC, USA) was used for all data analyses. Data were collected on days 5, 7 and 10 for any drug by dose by challenge-day (drug*dose*chalday) combination, meaning a multivariate response format. Initially, we transformed this multivariate into a univariate response format. For the nanoART uptake, the nanoART release and the antiretroviral activity, we used the mixed procedure in statistical analysis software to assess the effects of drug*dose*chalday (fixed effects) on antiretroviral response and to estimate their least-squares means (lsmeans), while treating the experimental unit within drug by dose (experimental unit [drug*dose]) as random effect. The lsmeans obtained from the data analyses were normalized in consideration of the positive control (infected MDM without nanoART treatments). Outcome was expressed relative to expression by positive controls (HIV-1 infection but no nanoART treatment), outcome as 100%, and negative controls (no infection or nanoART treatment), outcome as 0%. The Student's *t*-test was used to test the differences between the means of percent RT activity for two formulations at the same concentration. A p-value of 0.05 or less was considered significant.

Results

Manufacture & chemical characterization of nanoART

NanoART was manufactured as a nanosized drug crystal, prepared from free-base drug and coated with poloxamer and/or phospholipid surfactants with two notable exceptions. For EFV-2 and -3, the drug was first dissolved in a PLGA copolymer solution prior to NP preparation. For all, the physical properties of nanosuspensions differed substantively by size

and charge (Table 1). The NP ζ-potential ranged from −34.0 mV for IDV-1 coated with Lipoid E80 to +15.5 mV for RTV-4 coated with DSPE-mPEG$_{2000}$, P-188 and DOTAP. The average size ranged from 200 nm for RTV-2 to 1060 nm for IDV-1. A range of sized particles was observed from the nanometer to micrometer range (data not shown). NanoART suspensions showed distinctive morphologies based upon manufacturing methods, drug and surfactant coating. IDV, RTV and EFV NP preparations, over a range of particle sizes and surfactants, were either ellipsoid, rod, cuboidal or spherical in shape with smooth surfaces (Figure 1A, B, D, E, G & H). IDV NPs, over a range of sizes and surfactants, were ellipsoid in shape and had distinct smooth surfaces (Figure 1A & B). RTV NPs were rod-shaped prisms with sharp and geometrically varied edges (Figure 1D & E). The morphology of EFV NPs differed depending on the manufacture method. EFV-1 NPs, produced by high-pressure homogenization, were cuboidal with distinct, sharp and geometric edges (Figure 1G), while EFV-3 NPs, produced by sonication, were spherical with distinct and smooth surfaces (Figure 1H). Transmission-electron microscopy of MDM cocultured with IDV-4, RTV-4 and EFV-3 demonstrated NP co-localization in the MDM cytoplasm with retention of each formulation's structural integrity after uptake into cells and are readily identifiable based on their distinctive shapes (Figure 1C, F & I, colored outlines). No such structures were observed in transmission-electron microscopy of untreated MDM (data not shown).

NP uptake & antiretroviral drug release

Next, we determined the effect of altering individual physical properties of the NPs on MDM uptake. Using IDV as a representative drug formulation, we altered coating, size and charge of the nanoformulations and tested cell uptake and secretion profiles for each at a constant concentration of 100 μM. We determined the effect of surfactant coating on uptake by comparing IDV-1, which was coated with Lipoid-E80, to IDV-2, which was coated with a combination of P-188 and DSPE-mPEG$_{2000}$ (Table 1). Significant differences ($p < 0.05$) were observed in uptake rate and drug concentration. Maximum uptake was observed at 8 h for IDV-1 and 12 h for IDV-2 (Figure 2A), and the absolute amount of intracellular IDV was 1.65-fold greater for IDV-2 (45.74 μg/1 × 10^6 cells) than for IDV-1 (27.71 μg/1 × 10^6 cells).

To substantiate the RP-HPLC findings, we assessed uptake kinetics in real-time by live confocal imaging. In these experiments, rDHPE-labeled nanoART were added to cultures containing green-labeled MDM. Sequential still images of live cells taken at timed intervals supported the drug uptake measures and also demonstrated that the cells were able to uptake IDV-2 at a much greater rate than IDV-1 (Figure 2B) (Supplementary videos 1 & 2; for full videos see online www.futuremedicine.com/toc/nnm/4/8). These data, taken together, show that both rate and absolute amount of nanoART uptake are affected by surfactant coating. Next, we determined the effect of particle size on MDM uptake by comparing IDV-2 (970 nm) to IDV-3 (430 nm), both coated with a combination of P-188 and DSPE-mPEG$_{2000}$ (Table 1). Significant differences ($p < 0.05$) were seen in both rate and extent of uptake amongst these two formulations (Figure 2A). Maximum uptake was observed at 8 h for IDV-2 and 24 h for IDV-3. The absolute amount of intracellular nanoART was 2.56-fold greater for IDV-2 (45.74 μg/1 × 10^6 cells) than for IDV-3 (17.88 μg/1 × 10^6 cells). These data demonstrate that particle size affects the rate and absolute amount of NP absorption.

Finally, we determined the effect of particle surface charge by comparing the uptake of IDV-2 (−24.4 mV) and IDV-4 (+15.0 mV) (Table 1). The rate of uptake was similar for both formulations as was the time of maximum uptake, 8 h (Figure 2A). Differences in the absolute amounts of intra-cellular NPs for IDV-2 (45.74 μg/1 × 10^6 cells) and IDV-4 (53.78 μg/1 × 10^6 cells) are illustrated (Figure 2A). These data support the idea that size and surfactant are important parameters that dictate cell uptake. Moreover, during the first 4 h of exposure to

nanoART, absorption varied depending on the physical properties of the different NP formulations (Figure 2B).

After verifying that alteration of the physical properties of IDV NPs affects MDM uptake, we determined whether these same parameters could be applied to EFV and RTV. Four different formulations of RTV were developed (Table 1). The RTV formulation with the slowest rate and lowest absolute amount of uptake was RTV-1, which was coated with DSPE-mPEG$_{2000}$ alone, had a size of 200 nm and had a ζ-potential of −25.6 mV (Table 1). The RTV formulation with the fastest absorption rate and greatest accumulation of RTV was RTV-4, which was coated with a combination of P-188, DSPE-mPEG$_{2000}$ and DOTAP, had a size of 620 nm and had a ζ-potential of +15.5 mV. Maximum uptake occurred at 8 h for RTV-4 and at 12 h for RTV-1. Absolute amount of uptake was approximately 1.5-times greater for RTV-4 (40.98 μg/1 × 10^6 cells) than for RTV-1 (24.68 μg/1 × 10^6 cells) (Figure 3). The physical properties of RTV-4 were similar to IDV-4. This suggests that the physical properties that optimize the uptake of IDV NPs also optimize the uptake of RTV NPs. Three different formulations of EFV were synthesized (Table 1). The EFV formulation with the poorest uptake was EFV-1, which was coated with P-188 and DSPE-mPEG$_{2000}$, had a size of 600 nm and had a charge of −3.1 mV (Table 1). The formulation with the best uptake was EFV-3, which was encapsulated in PLGA, had a size of 300 nm, was coated with CTAB and had a charge of +7.4 mV (Table 1). Uptake of EFV-1 and -3 differed significantly in the absolute amount of uptake, but not in the rate (Figure 3). Maximum uptake occurred at approximately 1 h for both formulations. Absolute amount of uptake for EFV-3 (3.19 μg/1 × 10^6 cells) was three-times greater than for EFV-1 (0.91 μg/1 × 10^6 cells). On the other hand, EFV-3 had a different surfactant coating and was smaller in size when compared with IDV-4 and RTV-4, but had greater overall uptake when compared with EFV-1. This suggests that the physical properties that optimize the uptake of nanoART are drug dependent.

Diverse release profiles were seen for each drug and formulation. The amount of drug still contained within the cells and released into the media was assessed. We compared two representative formulations for each drug that were tested for NP uptake. When comparing MDM treated with either IDV-1 or IDV-4, the cellular drug content differed significantly ($p < 0.05$) at all time points (Figure 3). No drug was detectable by day 11 in cells treated with IDV-1 while drug was readily present at day 15 for IDV-4 (1.61 μg/1 × 10^6 cells). Drug concentration within media also differed significantly ($p < 0.05$) from days 3 to 15 (Figure 3). No drug was detectable in the media by day 13 in cells treated with IDV-1 while drug was readily present in IDV-4 treated MDM (16.37 μg/ml).

When comparing MDM treated with either RTV-1 or -4 the drug content of both the cells and the media differed ($p < 0.05$) at all time points (Figure 3). Drug was present within the cells at day 15 for both RTV-1 (0.19 μg/1 × 10^6 cells) and RTV-4 (8.69 μg/1 × 10^6 cells). Drug was also present within the media at day 15 for both RTV-1 (0.28 μg/ml) and RTV-4 (11.62 μg/ml). For MDM treated with either EFV-1 or -3 the drug content of both cells and media differed ($p < 0.05$) at all time points measured (Figure 3). No drug was detectable by day 7 in cells treated with EFV-1 while drug was present, albeit at low levels, at day 15 in cells treated with EFV-3 (0.09 μg/1 × 10^6 cells). At day 15, drug was present within the media from cells treated with EFV-3 (0.3 μg/ml), but by day 13 no drug was detectable from cells exposed to EFV-1.

Evaluation of the functional properties of cell-loaded NPs

Next, we assessed whether cell function was affected in monocytes and MDM loaded with nanoART. In these experiments, we used alamarBlue as a quantitative, scalable and rapid assay for cell viability and proliferation. The alamarBlue reagents incorporate an oxidation–reduction indicator that both fluoresces and changes color in response to chemical reduction of growth medium resulting from cell growth. Thus, the intensity of the oxidation–reduction indicator is

proportional to cell growth and cell viability. Results show that each of the IDV NPs tested at the highest concentration used (100 μM) did not significantly change the viability of monocytes (Figure 4A) or MDM (Figure 4B). All RTV NP preparations also tested at 100 μM did not alter macrophage viability (Figure 4B) but decreased monocyte viability by 15% (Figure 4A). Although NP loading increased monocyte migration across artificial blood–brain barrier models for both IDV-4 and RTV-4, the increase was not statistically significant (Figure 4C).

Antiretroviral efficacy of nanoART preparations

To determine the *in vitro* antiretroviral effects of nanoART taken up by MDM, we treated cells with individual nanoART preparations at concentrations of 1, 10 and 100 μM for 12 h and challenged the cells with HIV-1_{ADA} at a multiplicity of infection of 0.01 infectious virus particles/cell at 1, 5, 10 and 15 days after drug treatment. The same formulations at the same concentrations used for uptake and release were tested for antiretroviral activities to ensure that the data sets could be compared. A dose-dependent effect for RT activity for IDV-4 at all time points examined was observed, while IDV-1 exhibited a potential dose-dependent response only on days 1 and 5 (Figure 5A). When used at 100 μM, significant differences ($p < 0.05$) between the two formulations were observed starting on day 5 (Figure 5A). By day 15, IDV-1 treatment groups were not different from infected controls, while IDV-4 treatment groups maintained significant ($p < 0.05$) viral suppression (Figure 5A). Comparison of RT activity suppression activity for RTV-1 and -4 revealed potential dose–response trends for both drugs at all time points (Figure 5B). Reduced RT activity was maintained over time for cells treated with RTV-4 but not for cells treated with RTV-1. By day 15, RTV-1 showed a 34.84% reduction in RT activity compared with controls, while RTV-4 suppressed RT activity by 98.42% (Figure 5B). Comparison of EFV formulations yielded an apparent dose–response effect for EFV-3 on days 10 and 15 but not for EFV-1 (Figure 5C). Starting on day 5 and continuing through to day 15, significant differences ($p < 0.05$) between EFV-1 and -3 were seen at all treatment concentrations except for the 1 μM treatment group on day 15 (Figure 5C). By day 10 all treatment groups for EFV-1 were not significantly different from infected controls, while cells treated with 100 and 10 μM of EFV-3 induced significant ($p < 0.05$) viral suppression until day 15 (Figure 5C). Differences between total measured RT activities over 2 weeks are shown for cells treated with 100 μM of IDV-1, RTV-1 and EFV-1 compared with cells treated with the same concentration of IDV-4, RTV-4 and EFV-3 (Figure 5D & E).

Expression of HIV-1 p24 antigen was also used to substantiate antiretroviral activity in MDM that were treated with nanoART and subsequently infected with HIV-1. Evaluation of p24 expression by infected MDM treated with IDV-1 and IDV-4 showed a dose–response effect in the expression of p24 at all time points for cells treated with IDV-4 but only on day 1 for cells treated with IDV-1 (Figure 6). Significant differences ($p < 0.05$) between the two formulations were seen at all concentrations starting at day 1 (Figure 6). On day 15 cells treated with 100 μM of IDV-1 did not differ from infected controls, while those treated with 100 μM of IDV-4 showed significant differences ($p = 0.0003$) (Figure 6). Comparison of HIV-1 p24 antigen density in groups treated with RTV-1 or -4 showed potential dose–response effects at all time points for both formulations at all concentrations (Figure 6). Significant differences ($p = 0.0156$) in the density of HIV-1 p24 were observed starting on day 1 for cells treated with 100 μM of RTV NPs (Figure 6). By day 15, all treatment concentrations differed significantly between RTV formulations ($p < 0.021$) (Figure 6). When HIV-1 p24 expression was compared amongst groups treated with EFV-1 and -3, significant differences were seen at day 5 for cells treated with 10 μM of EFV nanoformulations ($p = 0.0317$) (Figure 6). By day 10, both formulations at all concentrations differed significantly ($p < 0.0001$) (Figure 6). While there was a gradual loss of viral inhibition by cells treated with EFV-1, viral suppression by cells treated with 100 μM of EFV-3 was maintained up to 15 days ($p = 0.0001$) (Figure 6). Overall, IDV-4, RTV-4 and EFV-3 inhibited HIV-1 progeny virion production in infected cells for 15

days, while IDV-1, RTV-1 and EFV-1 did not. This was demonstrated by the gradual loss of p24 inhibition as well as the breakthrough of viral spread over time as demonstrated by increased density of p24 labeling. This data set mirrors that of the RT analysis and demonstrates decreased rates of viral replication for IDV-4, RTV-4 and EFV-3 by showing reductions in both RT activity and HIV-1p24 over time.

Discussion

The HIV-1 pandemic continues to grow. An estimated 33.2 million people globally are infected with the virus; 2.2 million deaths occurred in 2008 alone, with the majority coming from the resource-limited areas [15,16]. The requirement for uninterrupted daily dosing, suboptimal patient adherence and inadequate tissue penetration continue to lead to treatment failure in a proportion of patients receiving ART [1,26]. Thus, our research effort in ART delivery has focused on developing long-acting parenteral drug formulations that can be maintained inside cells for periods measured in weeks and that travel specifically to viral sanctuaries [17–19, 27].

Using poorly water-soluble ART, we manufactured nanosuspensions by homogenization and/or sonication techniques, and studied, in a complete manner, the physical properties of nanoART including size, charge and surface coating. We now demonstrate that we are able to directly modify the pharmacokinetics and cellular handling of drugs by altering the physical properties of NP. Most importantly, we demonstrated proof of concept in that cells pretreated with nanoART release the drug and inhibit HIV-1 infection for up to 15 days after treatment.

Macrophage-based nanomedicine delivery has a number of advantages for ART in an infected human host, including drug stability, delivery into viral sanctuary sites and sustained release. First, oral administration of drugs shows limited biodistribution and commonly results in the development of viral sanctuaries. This can increase the rate of viral mutation, affect drug resistance and result in treatment failure [2–4]. In addition, inadequate penetration of ART drugs into the genital tract raises concern about the ongoing risk of transmission, even when plasma HIV RNA levels are below the limit of detection [28,29]. Second, once the NPs gain entry into the monocyte or MDM, the cells can hold the drug in an active and stable form for periods of weeks. As such, they could provide a means to improve dosing schedules, adherence to therapy and the therapeutic index. Third, since the very same cell that carries the virus throughout the body is being used to deliver drug, it is likely that suitable drug concentrations could reach tissue sites that otherwise would have little or no drug penetration. Indeed, we posit that such a drug-delivery system using highly stable nanoART specifically targeted to monocytes and macrophages could greatly improve therapeutic outcomes.

These studies are but an incremental advance from what is being realized for nanomedicine. Indeed, nanotechnology has revolutionized pharmacology and drug delivery [30–32]. NPs can be altered in size, shape and composition to allow incorporation of drugs with a variety of biochemical properties. In addition, formulating drugs as NPs can allow for cellular transport and delivery. MDM have been shown to be potential drug vehicles for uptake, transport and delivery of nanoART [17–19]. Based on known limitations, a broad range of methods was previously employed to incorporate ART drugs into nanocarriers, including mannosylated gelatin, squalenoyl NP, fullerene cages and polymeric nanogels [33–37]. However, in all cases, cellular uptake and release of the drug was either limited or complicated by toxicity. A recent report demonstrated that sustained plasma concentrations of ART could be achieved over weeks to months, but this required intramuscular or subcutaneous administrations [38]. Indeed, in our own work, using intravenous routes of injection, the absolute level of cellular uptake and distribution hindered the system. Therefore, *in vitro* treatment with nanoART followed by adoptive transfer was required [17,18]. This poses a challenge concerning the use of nanoART

in the clinic. In order to overcome this and other barriers, our laboratories have designed highly stable nanoART to specifically target monocytes and MDM, maximize cellular uptake and extend antiretroviral activity. Comparisons between results obtained in this cell-based system with *in vivo* drug distribution are currently ongoing in our laboratories.

The successful application of depot-injected risperidone in clinical practice demonstrated the benefits provided by long-acting drug therapies [39–42]. Risperidone is an example of a drug that successfully transferred from daily oral administration to a sustained depot injection. Similar to the present situation, depot injection of risperidone was a modification of a clinically accepted oral therapy. The use of this and other long-acting antipsychotic compounds improved dosing schedules, enhanced treatment adherence and improved treatment outcomes. We propose using nanoART for cell-based drug delivery to create a similar long-acting drug treatment for HIV infection. If nanoART could be manufactured to be stable, actively taken up by cells, transported into tissue and slowly released, then injectable long-acting antiretroviral nanoformulations, which we are in the process of developing, could be realized for translational studies.

Nanosized drug crystals coated with a mixture of surfactants enhanced cellular uptake and maximized time of drug release. By modifying the size, coating and charge of nanoART, we have determined important physical characteristics that greatly enhance the pharmacokinetics and cellular handling of nanoART. We determined that nanoART, which are approximately 1 μm in size, are taken up most rapidly. It has been shown that larger NPs are taken up in greater amounts by MDM compared with smaller particles [43–45]. This could potentially be due to the mechanism of uptake. Particles 1 μm or greater in size are generally taken up by phagocytosis, as opposed to smaller particles 300 nm or less, which are taken in by a pinocytotic-like mechanism such as clathrin/caveolae-mediated uptake [44,45].

We also determined that the surfactant used to coat nanoART greatly affects how cells handle them. It has been demonstrated that the coating of a NP can greatly affect cellular handling and stability [46–48]. In this study, a combination of DSPE-mPEG$_{2000}$ and P-188 was optimal for IDV and RTV. However, EFV uptake and release was much greater when it was encapsulated with PLGA. This demonstrates that there may be an optimal single or combination of surfactants for each ART drug that best maximizes uptake and release by cells. We also determined that positively charged nanoART are taken up better than negatively charged ones; although the difference is slight, this parallels previous findings [49].

Most important was the demonstration of the antiretroviral potential of nanoART. Cells pretreated with nanoART were protected against viral challenge for up to 15 days. Not only can cells actively take up nanoART, but they can also maintain the particles for long periods of time and allow steady release of drugs in clinically significant amounts.

Conclusion

The data contained in this report take us one step closer to realizing our goal of the synthesis of long-acting, injectable nanoformulated ART for human use. The potential benefits of such therapies for patient compliance and improved disease outcomes are significant. Moreover, such a method of drug delivery could also limit many of the untoward side effects of ART currently seen with oral therapy. Overall, the maintenance of consistent therapeutic plasma drug concentrations, which could allow for simpler dosing schedules, reduce the rates of viral mutation and disease progression, combat virus in hidden sanctuaries and improve treatment adherence. Linking these observations to what can occur *in vivo* after nanoART parenteral injections remains the singular focus of our laboratories research pursuits.

Future perspective

The precise mechanisms of uptake and release of nanoART are being pursued. This would address questions on particle trafficking within the cell compartments and resolve the query of how nanoART can be maintained inside macrophages and secreted slowly over defined time periods. It would also determine whether there are subpopulations of macrophages that are more amenable to such cell carriage. The linkages between *in vitro* observations and *in bivo* pharmacokinetics, biodistribution and antiretroviral properties are required. This will ultimately translate the potential use of nanoART as a new drug-delivery system for HIV-1-infected people.

Executive summary

HIV & antiretroviral therapy

- The number of people infected with HIV continues to grow with drug availability still limited in resource-limited settings.
- Patience compliance, notably in drug-abusing populations, is often limited. Therefore, finding effective long-term treatments is important.
- Antiretroviral therapy has greatly reduced the morbidity and mortality associated with HIV infection.
- HIV therapy has a number of limitations including side effects of the drugs, poor pharmacokinetics and tissue biodistribution.
- Failure of HIV therapy is common and linked to viral mutation, toxicity, compliance and biodistribution. These may be avoided by improving compliance and through maintaining sustained drug levels above an effective dose.

Nanomedicine & cell-mediated drug delivery

- Antiretroviral medications of low solubility can be manufactured by high-pressure homogenization into solid-crystalline nanoparticles (nanoART) stabilized by specific surfactants and polymers.
- NanoART can be formulated for uptake, transport and release by monocytes and tissue macrophages.
- The physical properties of nanoART affect the way the drug is handled by macrophages.
- By modifying size, charge and surfactant coating, the rate and amount of nanoART uptake into macrophages and the period of drug release can be significantly affected.
- NanoART are taken up and released by macrophages in clinically relevant amounts with limited cytotoxicity or loss of functional abilities. The drug is detectable in both cells and culture fluids for up to 15 days after particle exposure.
- Macrophages loaded with nanoART are capable of crossing the blood-brain barrier.
- Cells that have taken up nanoART demonstrate little to no infection after viral challenge up to 15 days post-nanoART treatment.

NanoART & HIV therapy

- Cell-mediated delivery of antiretroviral compounds could significantly improve HIV therapies.

- Delivering antiretroviral drugs, in the form of nanoART, to viral sanctuaries could eliminate viral reservoirs.
- Formulating antiretroviral compounds into nanoART could increase drug circulation time and improve treatment schedules by reducing the frequency of drug administration.
- Each antiretroviral medication may have a different surfactant, polymer or combination that will maximize uptake by macrophages.
- Further exploration of cell-uptake mechanisms and trafficking of nanoART by macrophages are needed to study the interactions between nanoART and cells.
- Animal studies are necessary to study the *in vivo* distribution and circulation time.

Supplementary Material

Refer to Web version on PubMed Central for supplementary material.

Acknowledgments

The authors thank R Taylor for critical reading of the manuscript and outstanding graphic and literary support. N Anderson's support for video editing and formatting is appreciated.

Financial & competing interests disclosure The work was supported by grants 2R01 NS034239, 2R37 NS36126, P01 NS31492, P20RR 15635, P01MH64570, and P01 NS43985 (to HE Gendelman) from the NIH and a grant from Baxter Healthcare in nanomedicine. S Graham, M Chaubal, J Werling and B Rabinow are employees of Baxter Healthcare Corporation who developed the nanoART formulations used in this article. The authors have no other relevant affiliations or financial involvement with any organization or entity with a financial interest in or financial conflict with the subject matter or materials discussed in the manuscript apart from those disclosed.

Bibliography

1. Hawkins T. Appearance-related side effects of HIV-1 treatment. AIDS Patient Care STDS 2006;20 (1):6–18. [PubMed: 16426151]
2. Shehu-Xhilaga M, Tachedjian G, Crowe SM, Kedzierska K. Antiretroviral compounds: mechanisms underlying failure of HAART to eradicate HIV-1. Curr. Med. Chem 2005;12(15):1705–1719. [PubMed: 16029143]
3. Delaugerre C, Peytavin G, Dominguez S, et al. Virological and pharmacological factors associated with virological response to salvage therapy after an 8-week of treatment interruption in a context of very advanced HIV disease (GigHAART ANRS 097). J. Med. Virol 2005;77(3):345–350. [PubMed: 16173015]
4. Duval X, Peytavin G, Albert I, et al. Determination of indinavir and nelfinavir trough plasma concentration efficacy thresholds according to virological response in HIV-infected patients. HIV Med 2004;5(4):307–313. [PubMed: 15236622]
5. Hammer SM, Eron JJ Jr, Reiss P, et al. Antiretroviral treatment of adult HIV infection: 2008 recommendations of the International AIDS Society-USA panel. JAMA 2008;300(5):555–570. [PubMed: 18677028]
6. Epstein LG, Gendelman HE. Human immunodeficiency virus type 1 infection of the nervous system: pathogenetic mechanisms. Ann. Neurol 1993;33(5):429–436. [PubMed: 8498818]
7. Best BM, Letendre SL, Brigid E, et al. Low atazanavir concentrations in cerebrospinal fluid. AIDS 2009;23(1):83–87. [PubMed: 19050389]
8. Pathan SA, Iqbal Z, Zaidi SM, et al. CNS drug delivery systems: novel approaches. Recent Pat. Drug Deliv. Formul 2009;3(1):71–89. [PubMed: 19149731]
9. Varatharajan L, Thomas SA. The transport of anti-HIV drugs across blood-CNS interfaces: summary of current knowledge and recommendations for further research. Antiviral Res 2009;82(2):A99–A109. [PubMed: 19176219]

10. Murri R, Lepri AC, Cicconi P, et al. Is moderate HIV viremia associated with a higher risk of clinical progression in HIV-infected people treated with highly active antiretroviral therapy: evidence from the Italian cohort of antiretroviral-naive patients study. J. Acquir. Immune Defic. Syndr 2006;41(1): 23–30. [PubMed: 16340469]
11. Alos L, Navarrete P, Morente V, et al. Immunoarchitecture of lymphoid tissue in HIV-infection during antiretroviral therapy correlates with viral persistence. Mod. Pathol 2005;18(1):127–136. [PubMed: 15389256]
12. Paterson DL, Swindells S, Mohr J, et al. Adherence to protease inhibitor therapy and outcomes in patients with HIV infection. Ann. Intern. Med 2000;133(1):21–30. [PubMed: 10877736]
13. Bruce RD, McCance-Katz E, Kharasch ED, Moody DE, Morse GD. Pharmacokinetic interactions between buprenorphine and antiretroviral medications. Clin. Infect. Dis 2006;43(Suppl 4):S216–S223. [PubMed: 17109308]
14. Bruce RD, Altice FL, Gourevitch MN, Friedland GH. Pharmacokinetic drug interactions between opioid agonist therapy and antiretroviral medications: implications and management for clinical practice. J. Acquir. Immune Defic. Syndr 2006;41(5):563–572. [PubMed: 16652030]
15. Chulamokha L, DeSimone JA, Pomerantz RJ. Antiretroviral therapy in the developing world. J. Neurovirol 2005;11(Suppl 1):76–80. [PubMed: 15960241]
16. De Cock K, Grubb I. Towards universal access: WHO's role in HIV prevention, treatment and care. Bull. World Health Organ 2006;84(7):506. [PubMed: 16878214]
17. Dou H, Destache CJ, Morehead JR, et al. Development of a macrophage-based nanoparticle platform for antiretroviral drug delivery. Blood 2006;108(8):2827–2835. [PubMed: 16809617]
18. Dou H, Morehead J, Destache CJ, et al. Laboratory investigations for the morphologic, pharmacokinetic, and anti-retroviral properties of indinavir nanoparticles in human monocyte-derived macrophages. Virology 2007;358(1):148–158. [PubMed: 16997345]
19. Gorantla S, Dou H, Boska M, et al. Quantitative magnetic resonance and SPECT imaging for macrophage tissue migration and nanoformulated drug delivery. J. Leukoc. Biol 2006;80(5):1165–1174. [PubMed: 16908517]
20. Gendelman HE, Kabanov A, Linder J. The promise and perils of CNS drug delivery: a video debate. J. Neuroimmune Pharmacol 2008;3(2):58. [PubMed: 18322803]
21. Gendelman HE, Orenstein JM, Martin MA, et al. Efficient isolation and propagation of human immunodeficiency virus on recombinant colony-stimulating factor 1-treated monocytes. J. Exp. Med 1988;167(4):1428–1441. [PubMed: 3258626]
22. Kalter DC, Greenhouse JJ, Orenstein JM, Schnittman SM, Gendelman HE, Meltzer MS. Epidermal Langerhans cells are not principal reservoirs of virus in HIV disease. J. Immunol 1991;146(10):3396–3404. [PubMed: 2026871]
23. Ahmed SA, Gogal RM Jr, Walsh JE. A new rapid and simple non-radioactive assay to monitor and determine the proliferation of lymphocytes: an alternative to [^{3}H]thymidine incorporation assay. J. Immunol. Methods 1994;170(2):211–224. [PubMed: 8157999]
24. Chaudhuri A, Yang B, Gendelman HE, Persidsky Y, Kanmogne GD. STAT1 signaling modulates HIV-1-induced inflammatory responses and leukocyte transmigration across the blood-brain barrier. Blood 2008;111(4):2062–2072. [PubMed: 18003888]
25. Chaudhuri A, Duan F, Morsey B, Persidsky Y, Kanmogne GD. HIV-1 activates proinflammatory and interferon-inducible genes in human brain microvascular endothelial cells: putative mechanisms of blood-brain barrier dysfunction. J. Cereb. Blood Flow Metab 2008;28(4):697–711. [PubMed: 17940540]
26. Fellay J, Boubaker K, Ledergerber B, et al. Prevalence of adverse events associated with potent antiretroviral treatment: Swiss HIV Cohort Study. Lancet 2001;358(9290):1322–1327. [PubMed: 11684213]
27. Dou H, Grotepas CB, McMillan JM, et al. Macrophage delivery of nanoformulated antiretroviral drug to the brain in a murine model of neuroAIDS. J. Immunol 2009;183(1):661–669. [PubMed: 19535632]
28. Swindells S, DiRienzo AG, Wilkin T, et al. Regimen simplification to atazanavir-ritonavir alone as maintenance antiretroviral therapy after sustained virologic suppression. JAMA 2006;296(7):806–814. [PubMed: 16905786]

29. McKinnon JE, Mellors JW, Swindells S. Simplification strategies to reduce antiretroviral drug exposure: progress and prospects. Antivir. Ther 2009;14(1):1–12. [PubMed: 19320232]
30. Kabanov AV, Gendelman HE. Nanomedicine in the diagnosis and therapy of neurodegenerative disorders. Prog. Polym. Sci 2007;32:1054–1082.
31. Kingsley JD, Dou H, Morehead J, Rabinow B, Gendelman HE, Destache CJ. Nanotechnology: a focus on nanoparticles as a drug delivery system. J. Neuroimmune Pharmacol 2006;1(3):340–350. [PubMed: 18040810]
32. Rabinow BE. Nanosuspensions in drug delivery. Nat. Rev. Drug Discov 2004;3(9):785–796. [PubMed: 15340388]
33. Couvreur P, Stella B, Reddy LH, et al. Squalenoyl nanomedicines as potential therapeutics. Nano Lett 2006;6(11):2544–2548. [PubMed: 17090088]
34. Vinogradov SV, Kohli E, Zeman AD. Cross-linked polymeric nanogel formulations of 5′-triphosphates of nucleoside analogues: role of the cellular membrane in drug release. Mol. Pharm 2005;2(6):449–461. [PubMed: 16323952]
35. Kuo YC. Loading efficiency of stavudine on polybutylcyanoacrylate and methylmethacrylate–sulfopropylmethacrylate copolymer nanoparticles. Int. J. Pharm 2005;290(1–2):161–172. [PubMed: 15664142]
36. Kuo YC, Chen HH. Entrapment and release of saquinavir using novel cationic solid lipid nanoparticles. Int. J. Pharm 2009;365(1–2):206–213. [PubMed: 18848610]
37. Jain SK, Gupta Y, Jain A, Saxena AR, Khare P. Mannosylated gelatin nanoparticles bearing an anti-HIV drug didanosine for site-specific delivery. Nanomedicine 2008;4(1):41–48. [PubMed: 18207463]
38. Baert L, van `t Klooster G, Dries W, et al. Development of a long-acting injectable formulation with nanoparticles of rilpivirine (TMC278) for HIV treatment. Eur. J. Pharm. Biopharm 2009;72(3):502–528. [PubMed: 19328850]
39. Rainer MK. Risperidone long-acting injection: a review of its long term safety and efficacy. Neuropsychiatr. Dis. Treat 2008;4(5):919–927. [PubMed: 19183782]
40. Taylor DM, Fischetti C, Sparshatt A, Thomas A, Bishara D, Cornelius V. Risperidone long-acting injection: a prospective 3-year ana lysis of its use in clinical practice. J. Clin. Psychiatry 2009;70(2): 196–200. [PubMed: 19026261]
41. Kane JM, Eerdekens M, Lindenmayer JP, Keith SJ, Lesem M, Karcher K. Long-acting injectable risperidone: efficacy and safety of the first long-acting atypical antipsychotic. Am. J. Psychiatry 2003;160(6):1125–1132. [PubMed: 12777271]
42. Altamura AC, Sassella F, Santini A, Montresor C, Fumagalli S, Mundo E. Intramuscular preparations of antipsychotics: uses and relevance in clinical practice. Drugs 2003;63(5):493–512. [PubMed: 12600227]
43. Beduneau A, Ma Z, Grotepas CB, et al. Facilitated monocyte–macrophage uptake and tissue distribution of superparmagnetic iron-oxide nanoparticles. PLoS ONE 2009;4(2):e4343. [PubMed: 19183814]
44. Vonarbourg A, Passirani C, Saulnier P, Simard P, Leroux JC, Benoit JP. Evaluation of pegylated lipid nanocapsules versus complement system activation and macrophage uptake. J. Biomed. Mater. Res. A 2006;78(3):620–628. [PubMed: 16779767]
45. Tabata Y, Ikada Y. Effect of the size and surface charge of polymer microspheres on their phagocytosis by macrophage. Biomaterials 1988;9(4):356–362. [PubMed: 3214660]
46. Mainardes RM, Gremiao MP, Brunetti IL, da Fonseca LM, Khalil NM. Zidovudine-loaded PLA and PLA–PEG blend nanoparticles: influence of polymer type on phagocytic uptake by polymorphonuclear cells. J. Pharm. Sci 2009;98(1):257–267. [PubMed: 18425813]
47. Gaucher G, Asahina K, Wang J, Leroux JC. Effect of poly(*N*-vinyl-pyrrolidone)-block-poly(D,L-lactide) as coating agent on the opsonization, phagocytosis, and pharmacokinetics of biodegradable nanoparticles. Biomacromolecules 2009;10(2):408–416. [PubMed: 19133718]
48. Sant S, Poulin S, Hildgen P. Effect of polymer architecture on surface properties, plasma protein adsorption, and cellular interactions of pegylated nanoparticles. J. Biomed. Mater. Res. A 2008;87 (4):885–895. [PubMed: 18228249]

49. Roser M, Fischer D, Kissel T. Surface-modified biodegradable albumin nano- and microspheres. II: effect of surface charges on *in vitro* phagocytosis and biodistribution in rats. Eur. J. Pharm. Biopharm 1998;46(3):255–263. [PubMed: 9885296]

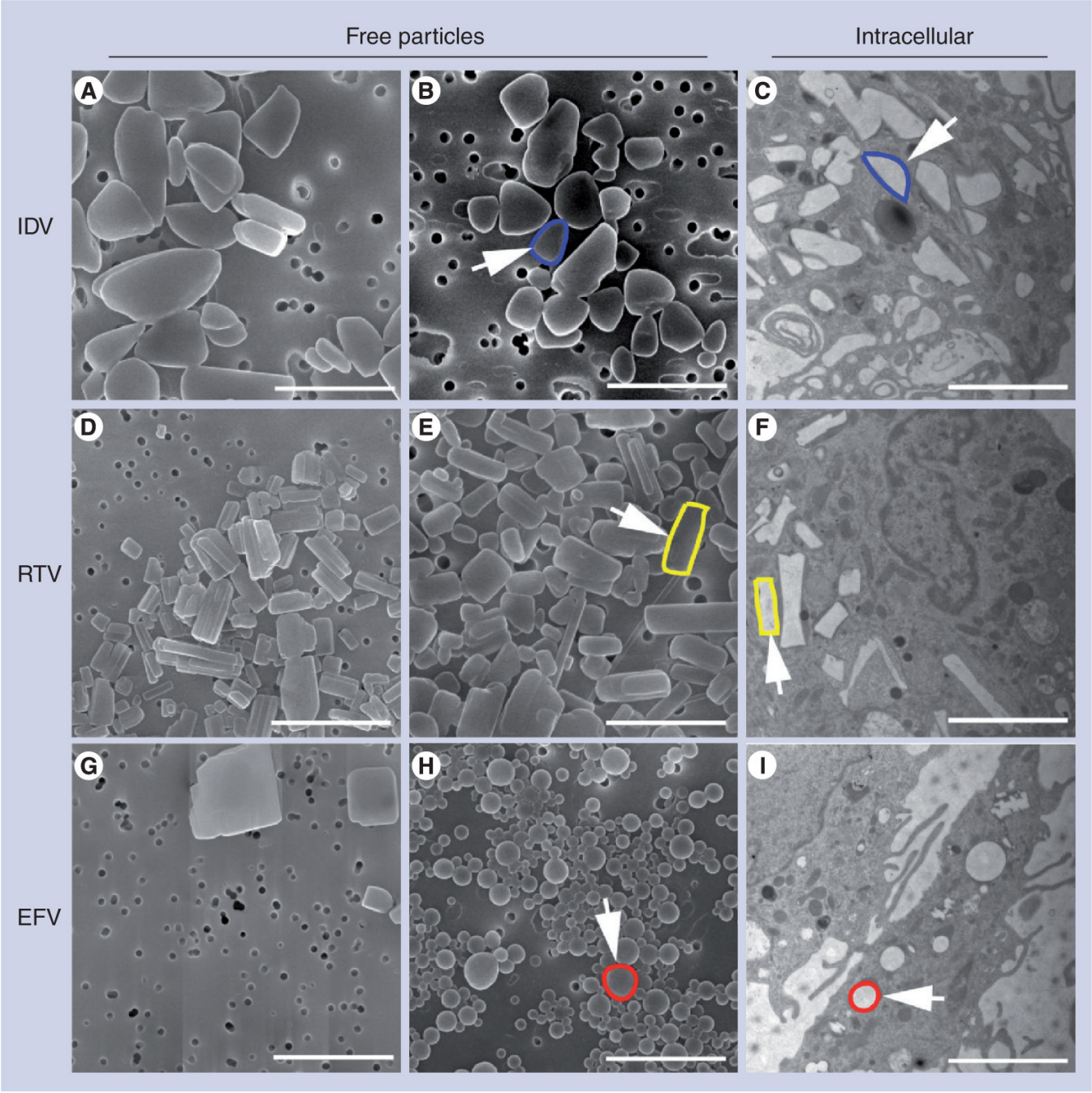

Figure 1. Nanoparticle morphology

Scanning-electron microscopy analysis (magnification: 15,000×) of nanoformulations shown include **(A)** IDV-1, **(B)** IDV-4, **(D)** RTV-1, **(E)** RTV-4, **(G)** EFV-1 and **(H)** EFV-3 on top of a 0.2 μm polycarbonate filtration membrane. Scale bar = 2.0 μm. **(A)** IDV-1 and **(B)** IDV-4 showed ellipsoid structures with sizes of approximately 1 μm; **(D)** RTV-1 and **(E)** RTV-4 showed rod structures with sizes of approximately 550 nm; **(G)** EFV-1 showed cuboidal structures with sizes of approximately 600 nm while **(H)** EFV-3 showed spherical structures with sizes of approximately 300 nm. Transmission-electron microscopy (magnification: 15,000×) demonstrated uptake of nanoART into monocyte-derived macrophages exposed to **(C)** IDV-4, **(F)** RTV-4 and **(I)** EFV-3. Within the cells, each type of nanoART is readily

identifiable by shape and an example has been outlined in blue for **(B & C)** IDV, yellow for **(E & F)** RTV and red for **(H & I)** EFV.
EFV: Efavirenz; IDV: Indinavir; RTV: Ritonavir.

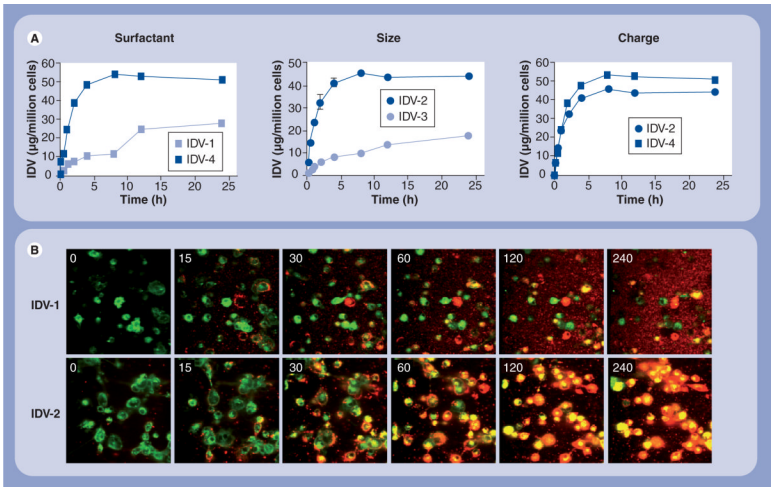

Figure 2. Uptake of indinavir nanoART into monocyte-derived macrophages

Data represent the means ± standard deviation for n = 3 determinations/time point. **(A)** Levels of IDV from cell lysates of cultured monocyte-derived macrophages treated with 100 μM nanoART and collected at specified times were assayed by reverse-phase high-performance liquid chromatography. The effect of particle size, charge and surfactant on uptake of nanoART was determined. **(B)** Fluorescent microscopy (time in min) of monocy-derived macrophages (green) labeled with Vybrant DiO cell-labeling solution and cocultured with 100 μM IDV nanoparticles (red) labeled with rhodamine B 1,2-dihexadecanoyl-sn-glycero-3-phosphoethanolamine, triethylammonium salt confirmed intracellular localization of nanoART and demonstrated the effect of surfactant coating on nanoparticle uptake.
IDV: Indinavir.

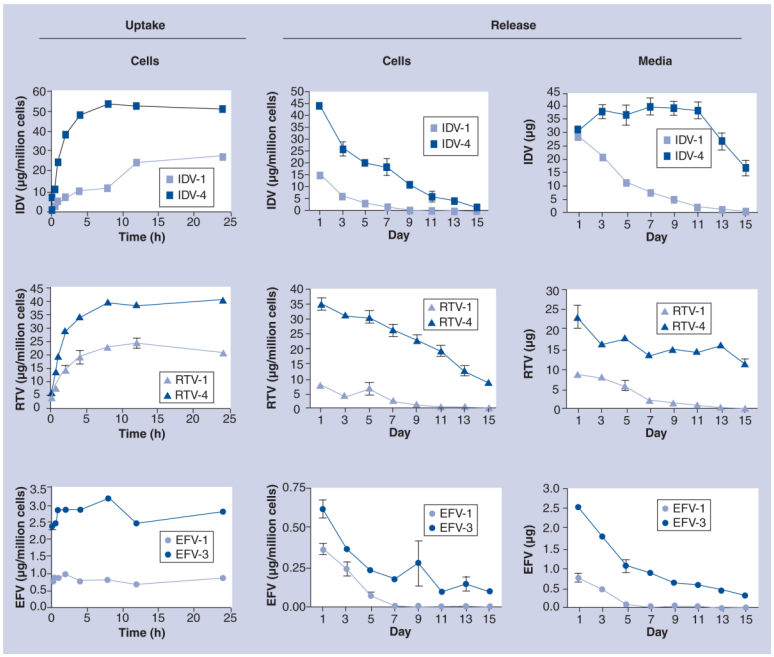

Figure 3. Uptake and release of indinavir, ritonavir and efavirenz nanoART from monocyte-derived macrophages

Data represent the means ± standard deviation for n = 3 determinations/time point. (Uptake) Levels of IDV, RTV or EFV from cell lysates of cultured monocyte-derived macrophages treated with 100 μM nanoART and collected at specified times were assayed by reverse-phase high-performance liquid chromatography. (Release) Levels of IDV, RTV or EFV were assayed over 15 days by reverse-phase high-performance liquid chromatography from cell lysates of cultured monocyte-derived macrophages treated with nanoART (cells) and extracellular media (media) at specified times.

EFV: Efavirenz; IDV: Indinavir; RTV: Ritonavir.

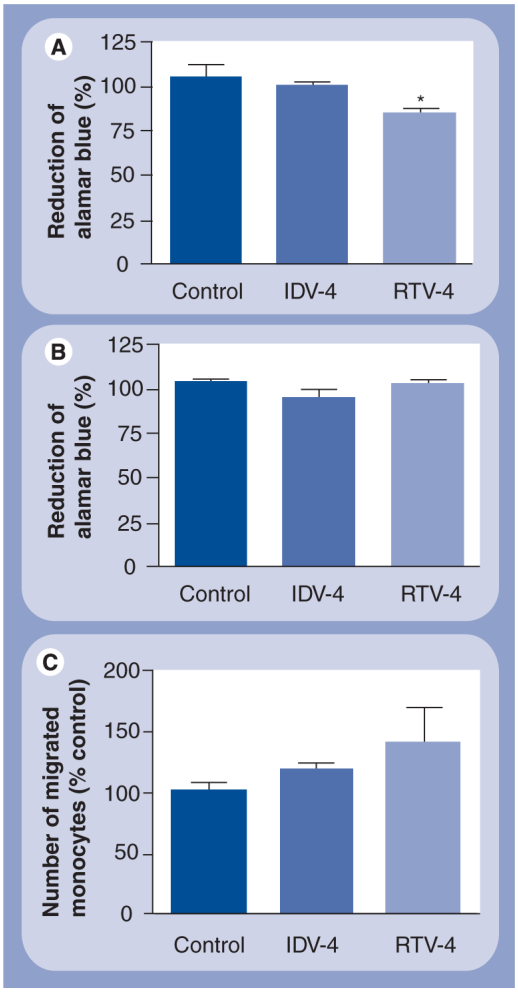

Figure 4. Effect of nanoART loading on monocyte and macrophage viability and blood–brain barrier migration

Data represent the means ± standard deviation for n = 3 determinations/treatment. **(A)** Monocytes and **(B)** monocyte-derived macrophages were loaded with 0.1 mM IDV-4 or RTV-4 and cell viability assessed 24 h later by the alamarBlue™ assay. At 0.1 mM concentration, IDV-4 did not significantly alter monocyte or macrophage viability, but RTV-4 decreased monocyte viability by approximately 20% ($p < 0.05$). At 0.1 mM concentration, both IDV-4 and RTV-4 increased monocyte migration across *in vitro* blood–brain barrier model **(C)**, but the increase was not statistically significant. Control represents monocytes or monocyte-derived macrophages not loaded with nanoparticles.

IDV: Indinavir; RTV: Ritonavir.

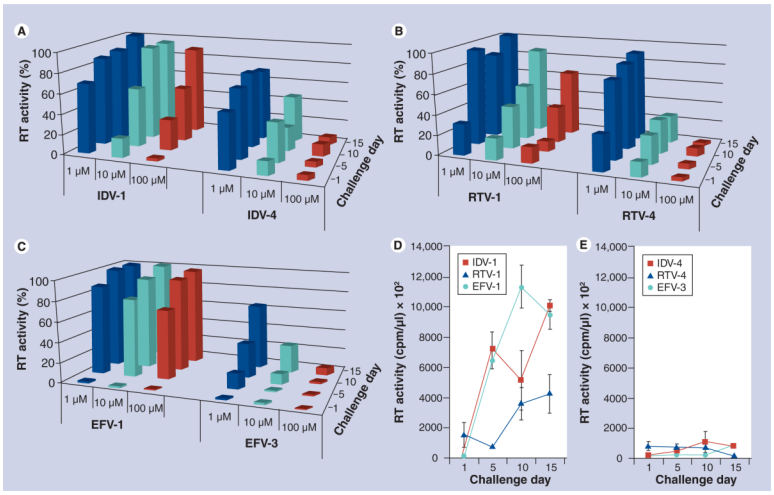

Figure 5. NanoART effects progeny virion release from virus-infected monocyte-derived macrophages

Comparison of antiretroviral effects of **(A)** IDV-1 versus IDV-4, **(B)** RTV-1 versus RTV-4 and **(C)** EFV-1 versus EFV-3 over 15 days in monocyte-derived macrophages pretreated with 1, 10 or 100 μM of nanoART, as measured by RT activity and normalized to infected control cells. RT activities as measured by ^{3}H-TTP incorporation for infected monocyte-derived macrophages treated with **(D)** IDV-1, RTV-1 and EFV-1, and **(E)** IDV-4, RTV-4 and EFV-3. Data represent the least squared means for n = 3 determinations/treatment.

EFV: Efavirenz; IDV: Indinavir; RT: Reverse transcriptase; RTV: Ritonavir.

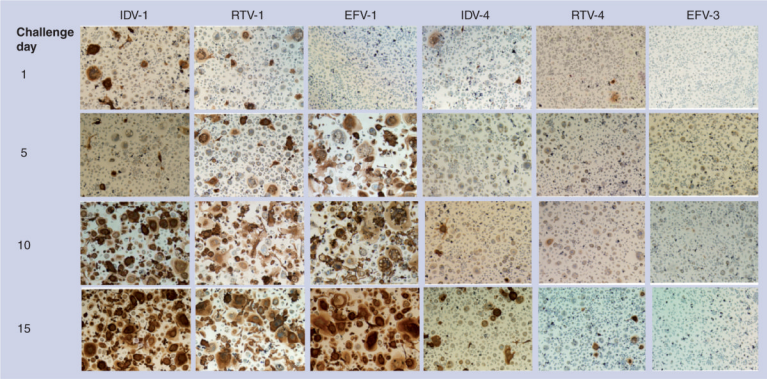

Figure 6. NanoART effects on HIV-1 p24 antigen expression

Comparison of antiretroviral effect of IDV-1 to ID-4, RTV-1 to RTV-4, EFV-1 to EFV-3 over 15 days in monocyte-derived macrophages pretreated with 100 μM of nanoART. A total of 10 days after each viral challenge cells were immunostained for HIV-1p24 antigen (brown). Three photos at a magnification of 4× from each well were quantified by densitometry using Image-Pro Plus, v. 4.0. Expression of p24 was quantified by determining the positive area (index) as a percentage of the total image area per microscopy field. Data represent least squares means of n = 3 determinations/time point. Cells treated with IDV-1, RTV-1 or EFV-1 showed progressive loss of antiretroviral protection and increased HIV p24 expression over time, while cells treated with IDV-4, RTV-4 or EFV-3 showed complete or near complete suppression of viral p24 production.

EFV: Efavirenz; IDV: Indinavir; RTV: Ritonavir.

Table 1

Physical characteristics of manufactured antiretroviral nanoparticles.

Formulation	Drug	Surfactant	Size (nm)	ζ-potential
IDV-1	IDV	Lipoid E80	1060	−34.0
IDV-2	IDV	P-188, DSPE-mPEG$_{2000}$	970	−24.4
IDV-3	IDV	P-188, DSPE-mPEG$_{2000}$	430	−21.6
IDV-4	IDV	P-188, DSPE-mPEG$_{2000}$ DOTAP	980	+15.0
IDV-5	IDV-p	P-188, DSPE-mPEG$_{2000}$	1400	−31.0
IDV-6	IDV-p	P-188, Tween® 80	1600	−29.5
RTV-1	RTV	DSPE-mPEG$_{2000}$	200	−25.6
RTV-2	RTV	DSPE-mPEG$_{2000}$	500	−21.1
RTV-3	RTV	P-188, DSPE-mPEG$_{2000}$	600	−26.2
RTV-4	RTV	P-188, DSPE-mPEG$_{2000}$, DOTAP	620	+15.5
EFV-1	EFV	P-188, DSPE-mPEG$_{2000}$	600	−3.1
EFV-2	EFV	PLGA	290	−1.3
EFV-3	EFV	PLGA, CTAB	300	+7.4

CTAB: Cetyltrimethyl ammonium bromide; DOTAP: (1-oleoyl-2-[6-[(7-nitro-2-1,3-benzoxadiazol-4-yl) amino]hexanoyl]-3-trimethylammonium propane); DSPE: 1,2-distearoyl-phosphatidyl-ethanolamine; EFV: Efavirenz; IDV: Indinavir; IDV-p: IDV-pamoate; mPEG: Methyl-poly(ethylene-glycol); P-188: Poloxamer 188; PLGA: Poly(lactic-co-glycolic acid); RTV: Ritonavir.